Application of Mg-Mesoporous Alumina Prepared by Using Magnesium Stearate as a Template for the Removal of Nickel: Kinetics, Isotherm, and Error Analysis

ARTICLE *in* INDUSTRIAL & ENGINEERING CHEMISTRY RESEARCH · APRIL 2007

Impact Factor: 2.59 · DOI: 10.1021/ie060994n

4 AUTHORS, INCLUDING:

Rengaraj Selvaraj
Sultan Qaboos University
57 PUBLICATIONS **2,709** CITATIONS
SEE PROFILE

Jei-Won Yeon
Korea Atomic Energy Research Institute (KAE…
52 PUBLICATIONS **347** CITATIONS
SEE PROFILE

Application of Mg-Mesoporous Alumina Prepared by Using Magnesium Stearate as a Template for the Removal of Nickel: Kinetics, Isotherm, and Error Analysis

Selvaraj Rengaraj,*,† Jei-Won Yeon,† Younghun Kim,‡ and Won-Ho Kim†

Nuclear Chemistry Research Division, Korea Atomic Energy Research Institute, Daejeon 305-353, South Korea, and Department of Chemical Engineering, Kwangwoon University, Seoul 139-701, South Korea

A new and novel adsorbent of Mg-mesoporous alumina prepared via a templating method was used to adsorb nickel from aqueous solution. The adsorption mechanism is assumed to be an ion exchange between Ni(II) and magnesium ion present on the surface of the newly prepared mesoporous alumina. The sorption was examined in terms of its equilibria and its kinetics. The sorption data have been analyzed and fitted to the linearized adsorption isotherms of the Freundlich, Langmuir, Temkin, and Dubin−Redushkevich models. The kinetic studies showed that the sorption rates could be described well by a pseudo-second-order expression rather than by the more commonly applied Lagergren pseudo-first-order kinetic model. The best fitting of experimental results to the proposed isotherms was observed in models that assume that ionic species bind first at the energetically most favorable sites. The results show that Mg-mesoporous alumina holds great potential to remove Ni(II) species from aqueous solution because the ΔG value of Mg(II), which is present in mesoporous alumina, has a more negative value when compared with Ni ion.

1. Introduction

In recent years, increasing awareness of the environmental impact of heavy metals has prompted a demand for the purification of industrial waters prior to discharge into natural waters. Heavy metal ions from aqueous solutions are considered as hazardous pollutants because of their toxicity even at a low concentration. The removal of heavy metals from water and wastewater has become a very important environmental issue.[1,2] The nickel(II) concentration in wastewater from mine drainage, tableware plating, metal finishing, and forging was up to 130 mg/L.[3] In drinking water, nickel may cause health problems if found in amounts greater than the health standard set (MCLG = 0.1 mg/L) by the United States Environmental Protection Agency (EPA). The MCLG for nickel has been set at 0.1 parts per million (ppm) because the EPA believes this level of protection would not cause any of the potential health problem. A higher concentration of nickel causes cancer of lungs, nose, and bone. Nickel carbonyl has been estimated as lethal in humans at atmospheric exposure of 30 ppm for 30 min;[4] poisoning causes dizziness, headache, nausea and vomiting, chest pain, dry cough and shortness of breath, rapid respiration, cyanosis, and extreme weakness.[5] These harmful effects of Ni(II) necessitate its removal from wastewaters before release into streams.[6]

Conventional methods of Ni(II) removal from wastewaters, including ion exchange,[7] chemical precipitation,[8,9] coagulation/flocculation,[10] complexation/sequestration,[6] electrochemical operations,[6] biological treatment,[11] ultrafiltration, or electrochemical deposition, do not seem to be economically feasible for water and wastewater treatment because of their relatively high costs or difficulty to implement in developing countries. Therefore, the need exists for a treatment strategy that is simple and robust and that addresses local resources and constraints. Sorption operations, including adsorption and ion exchange, are a potential alternative for water and wastewater treatment. Adsorption has advantages over other methods. The design is simple, and it is sludge free and can involve low investment in terms of both the initial cost and land. The adsorption of heavy metals by inorganic materials such as silica, mica, kaolin, calcium carbonate, titanium dioxide, and alumina has received much attention owing to the latest development of more advanced skills and sophisticated equipment.[12,13] Mesoporous alumina has been recognized as a highly effective adsorbent for the treatment of heavy metals in wastewater. We have recently reported that mesoporous alumina removed arsenic and copper from aqueous solution.[14,15]

Conventional porous solids, such as clay, fly ash, activated carbon, and silica materials, have nonuniform pore structure and low adsorption capacities with slow adsorption kinetics. It suggests that an ideal adsorbent should have accessible interlinked pore structures with uniform pore-size distribution and high surface area with physical/chemical stability. Thus, no pore blocking occurs during adsorption with minimization of transparent resistance. Mesoporous alumina has a large surface area with uniform pore-size distribution and a spongelike interlinked pore system.[14,15] In addition, these mesoporous materials (silica and alumina) showed high uptake and stability as adsorbents. However, the preparation step requires an expensive chemical, stearic acid, for the structural agent. An alternative chemical is needed to have economic feasibility of mesoporous alumina for the practical application. Thus, a new preparation procedure was developed using magnesium stearate as a structural agent.[16] It should be noted that the cost of magnesium stearate is ∼70× less than that of stearic acid. Resulting materials showed high uptake and good stability for the nickel ion adsorption process.

The main objective of this research was prepared by using magnesium stearate, which is a salt of stearic acid and a cost-effective material to investigate the level of efficiency of activated alumina with a mesoporous structure as a possible adsorbent for the removal of Ni(II) from aqueous solutions and to investigate the ion-exchange mechanism.

2. Experimental Section

2.1. Synthesis of Mesoporous Alumina. Stearic acid was used as the anionic surfactant to synthesize mesoporous alu-

* To whom correspondence should be addressed. Tel.: +82-42-868-2465. Fax: +82-42-868-8148. E-mail: srengaraj1971@yahoo.com.

† Korea Atomic Energy Research Institute.

‡ Kwangwoon University.

10.1021/ie060994n CCC: $37.00
Published on Web 03/29/2007

minas, and aluminum *sec*-butoxide was used as an aluminum precursor via the posthydrolysis method.[17,18] The aluminum source and surfactant were dissolved separately in *sec*-butyl alcohol, after which the two solutions were then mixed. Small amounts of water were slowly added dropwise into the mixture at a rate of 1 mL/min, generating a white precipitate. This resulting suspension was further stirred for 24 h. The resulting materials were calcined for 3 h at 450 °C in air. The molar ratio of this reaction mixture was 1Al(*sec*-BuO)$_3$/0.2($C_{17}H_{35}$-COO)$_2$Mg/5*sec*-BuOH/4H_2O (within appropriate 1 M HNO_3). Aluminas prepared using magnesium stearate as templates are referred to as Mg-MA.

2.2. Characterization of Mesoporous Alumina. Fourier transform infrared (FT-IR) analysis was performed to confirm that the templates were removed from the as-made materials. Nitrogen adsorption/desorption experiments were carried out using a Micromeritics ASAP 2010 analyzer. The pore-size distributions were calculated using the Barret−Joyner−Halenda (BJH) method on the desorption branch. To analyze the crystallinity of the prepared samples, powder X-ray diffraction (XRD model M18 XHF-SRA, MAC/Science) patterns were recorded using Cu Kα radiation at 50 kV and 100 mA. The porosity of the calcined samples was characterized by transmission electron microscopy on a JEM-2000EXII instrument. Thermogravimetric analysis (TGA) patterns were collected on a Perkin-Elmer TGA-7 thermogravimetric analyzer in order to set calcination conditions. The adsorption capacities of nickel were measured by an inductively coupled plasma spectrophotometer (ICP) (ULTIMA 2−Jobin Yvon Horiba) for nickel content.

2.3. Batch-Mode Studies. A stock solution of nickel ions was prepared by dissolving the appropriate amount of $Ni(NO_3)_2 \cdot 6H_2O$ (Aldrich) in double-distilled water. The stock solution was diluted as required to obtain standard solutions containing 5−30 mg/L of Ni(II). Ni(II) solution (100 mL) of a desired concentration, adjusted to a desired pH, was taken in reaction bottles of 300 mL capacity, and known amounts of ion-exchange resins were added. The solutions were agitated with 150 rpm for a predetermined period at 25 ± 1 °C in a shaking incubator (JEIO TECH SI-900R). The mesoporous aluminas were separated, and the filtrate was analyzed by ICP for nickel content.

2.4. Isotherm Experiments. Adsorption isotherm studies were carried out with 100 mL of different initial Ni(II) concentrations while maintaining the mesoporous alumina dosage at a constant level. The initial concentrations of solutions taken for the studies were 5, 10, 15, 20, 25, and 30 mg/L. The equilibrium adsorption capacity was calculated using

$$q_e = \frac{(C_0 - C_e)V}{M} \tag{1}$$

where q_e (mg/g) is the equilibrium adsorption capacity, C_0 and C_e are the initial and equilibrium concentrations (mg/L) of nickel ions in solution, V (L) is the volume, and M (g) is the weight of the adsorbent.

2.5. Kinetic Studies. Kinetic experiments were conducted by using a known weight of mesoporous alumina dosage and employing Ni(II) concentration in the range of 10−30 mg/L. The samples at different time intervals (0−360 min) were taken and centrifuged. Suitable aliquots were analyzed for nickel concentration and recorded. The rate constants were calculated by using the conventional rate expression. The amount of metal ion sorbed, q_t, was calculated from

$$q_t = \frac{(C_0 - C_t)V}{M} \tag{2}$$

where q_t (mg/g) is the equilibrium adsorption capacity, C_0 and C_t are the initial and equilibrium concentration (mg/L) of nickel ions in solution, V (L) is the volume, and M (g) is the weight of the adsorbent.

3. Results and Discussion

3.1. Characterization of Mesoporous Alumina. 3.1.1. FT-IR Analysis of Mesoporous Alumina. Figure 1 represents the FT-IR characteristic results of MA, Mg-MA, and their templates (e.g., stearic acid and magnesium stearate). FT-IR results suggest that the formation mechanism using stearic acid salts, such as magnesium stearate, is the same as that when stearic acid is used as a chemical. The as-made alumina using stearic acid with sodium hydroxide gave a strong band at 1335−1440 cm^{-1}, assigned to symmetric $-COO^-$ stretching, and a band at 1550−1650 cm^{-1}, assigned to asymmetric $-COO^-$ stretching. This result implies that the carboxyl group ($-COOH$, 1700 cm^{-1}) of stearic acid was transformed into a carboxylic salt ($-COO^-$) in the solvent, after which the salts might have been combined with the aluminum precursor. The mechanism involved is similar to the mediated pathway through charge matching ($S^-M^+I^-$) when mesoporous silica was prepared using an ionic surfactant.[19,20] Therefore, different salts, such as magnesium stearate, can also be used as chemical templates for preparing mesoporous alumina via a charge-matching pathway.

3.1.2. Nitrogen Adsorption and Desorption. Figure 2 and Table 1 represent the pore-size distribution of MA and Mg-MA. The N_2 adsorption/desorption isotherm was a typical type of IV isotherm and an H_2 hysteresis loop, indicating mesoporous porosity.[21] The framework porosity at 0.4−0.7 P/P° in the N_2 isotherm indicates that the porosity is contained within the uniform channels of the templated framework, while the textural porosity at 0.8−1 P/P° is indicative of a porosity arising from noncrystalline intra-aggregate voids and spaces formed by interparticle contacts. MA and Mg-MA had a mainly framework porosity. Therefore, the pore properties of MA and Mg-MA are affected slightly by the type of surfactant used. However, both MA and Mg-MA have a similar pore size (3.6 nm) and narrow pore-size distribution ($D_{fwhm} \approx 1.0$ nm). Because the alkyl chain length of the surfactants is identical, the pore sizes are essentially the same.

3.1.3. XRD Analysis of Mesoporous Alumina. In low-angle XRD patterns for mesoporous aluminas, only one peak appeared at 2θ between 0.5−3°.[22] The generation of X-ray peaks results from a difference in the scattering power (or scattering contrast) between two building blocks (amorphous wall and pore channel contained with air and helium) of mesoporous materials. This indicates that the mesoporous aluminas have different pore structures compared to hexagonal mesoporous silicas such as MCM-41 or SBA-15, which exhibit three peaks at 2θ between 0.5−5°. Thus, the mesoporous aluminas prepared here have a spongelike pore-channel structure with a random pore distribution, whereas MCM-41 has a 1D cylindrical pore structure with a highly regular pore distribution. These results are consistent with the following TEM data (Figure 4).

Figure 3 represents the crystalinity of MA, Mg-MA, and Ni/Mg-MA. XRD patterns of MA and Mg-MA typically show the characteristic peaks of activated alumina. The pattern for Mg-MA was similar to that of MA, while the peaks position left-shifted and the width of the peaks became too narrow without any magnesium peaks. This is due to the characteristic peaks

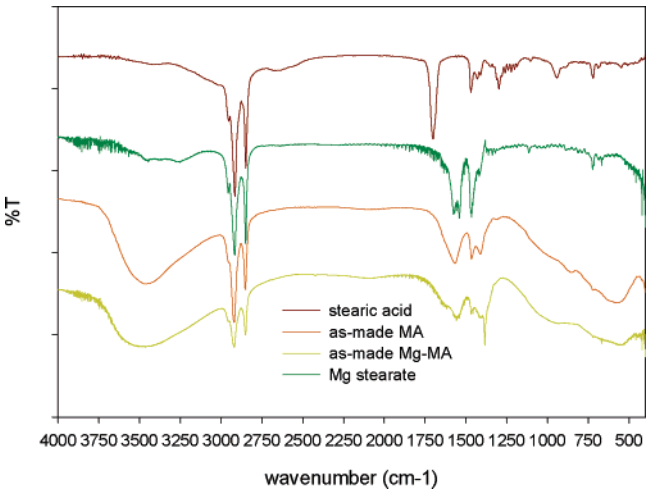

Figure 1. FT-IR pattern of mesoporous alumina.

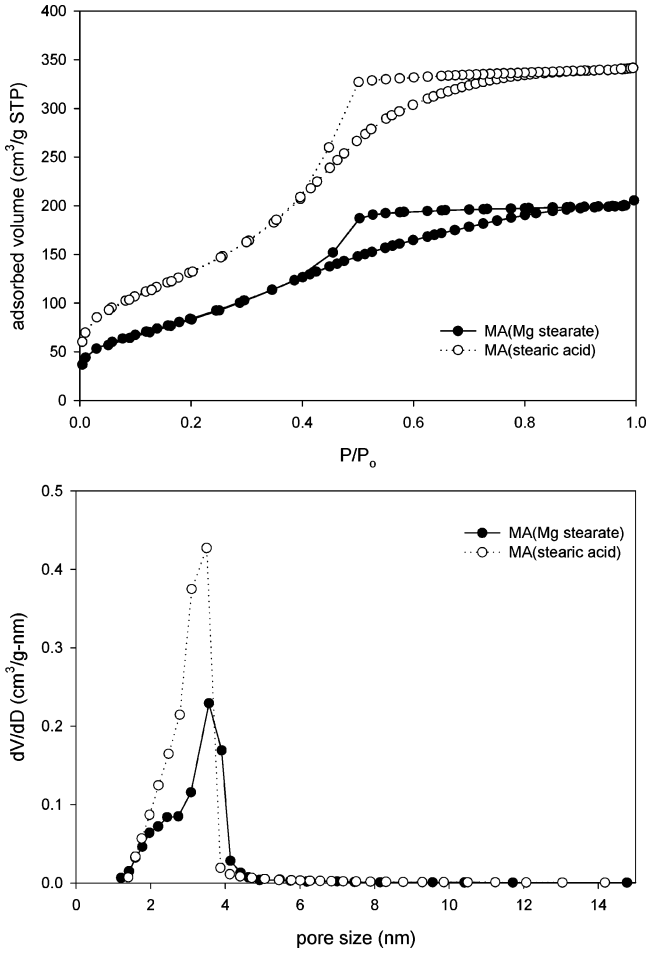

Figure 2. N_2 isotherm and pore-size distribution of MA and Mg-MA.

Table 1. Pore Properties of Prepared Mesoporous Aluminas

samples	template	D (nm)	D_{FWHM}[a] (nm)	S_{BET} (m^2/g)	V_P (cm^3/g)
MA	$C_{17}H_{35}COOH$	3.49	0.89	485	0.50
Mg-MA	$(C_{17}H_{35}COO)_2Mg$	3.56	1.03	311	0.31

[a] Full width at half-maximum of pore-size distribution.

of the magnesium spinel structure, which overlapped with that of the activated alumina phase. In addition, magnesium ions occupy the cation vacancy and reinforce the structure of alumina, and thus, the peak width is narrowed. After Ni adsorption using Mg-MA adsorbent, no peak shape of Ni/Mg-MA was changed as compared to that of Mg-MA. If nickel metal was loaded on the aluminas, characteristic peaks of nickel could be obtained.

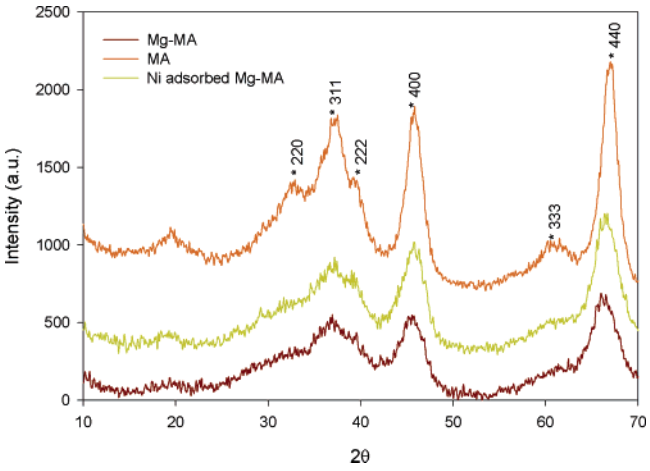

Figure 3. XRD patterns of MA, Mg-MA, and Ni/Mg-MA.

3.1.4. TEM Analysis of MA, Mg-MA, and Ni/Mg-MA. Figure 4 represents the TEM images of MA, Mg-MA, and Ni/Mg-MA. In all of the MA and Mg-MA, the developed framework pores had a spongelike appearance, which confirms the advantage of having an interconnected pore system. An interconnected pore structure has the advantage of a reduced diffusion limitation and an enhanced molecular accessibility to active sites on the inner surface. A similar pore morphology was found for disordered mesoporous silica and alumina when cationic or neutral surfactants were used in their preparation.

3.1.5. TGA Analysis of MA and Mg-MA. Figure 5 represents the TGA pattern of MA and Mg-MA. The TGA result of pure stearic acid shows two peak groups at the melting point and boiling point, while as-made aluminas show three broad peaks, at ~110 and 330 °C. The first peak corresponds to physically adsorbed water, and the second is stearic acid and dehydroxylation of the sample. Two sequential processes, that is, loss of water molecules by desorption of physically adsorbed water (110 °C) and condensation of adjacent surface or internal hydroxyl groups (220−420 °C), occurred during the dehydration/dehydroxylation of the prepared alumina.[14]

3.2. Equilibrium Studies. The salient features of isotherms are needed before the kinetics of the adsorption process is interpreted. The dynamic adsorptive separation of solute from solution onto an adsorbent depends upon a good description of the equilibrium separation between the two phases. Many models have been proposed to explain adsorption equilibria, but the most important factor is to have applicability over the entire range of process conditions. The most widely used isotherm models for solid−liquid adsorption are the Freundlich, Langmuir, Redlich−Peterson, Temkin, and Dubinin−Redushkevich isotherms.

The Freundlich isotherm model was also used to explain the observed phenomena.

$$\log q_e = \log K_F + n \log C_e \qquad (3)$$

where K_F is the Freundlich constant and n is the Freundlich exponent. K_F and n are constants incorporating all factors affecting the adsorption process such as adsorption capacity and intensity. Linear plots of log q_e vs log C_e shows that the adsorption follows the Freundlich isotherm model. K_F and n were calculated from the intercept and the slope of the plot.

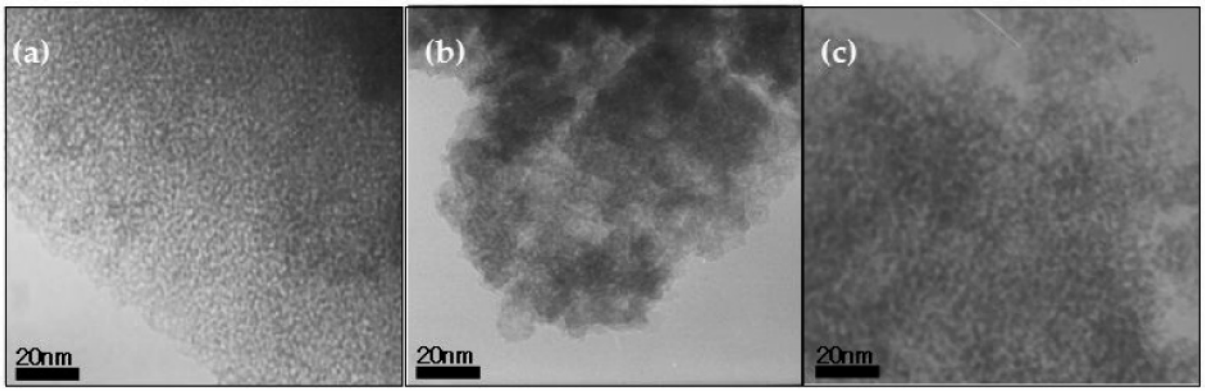

Figure 4. TEM images of (a) MA, (b)Mg-MA, and (c) Ni/Mg-MA.

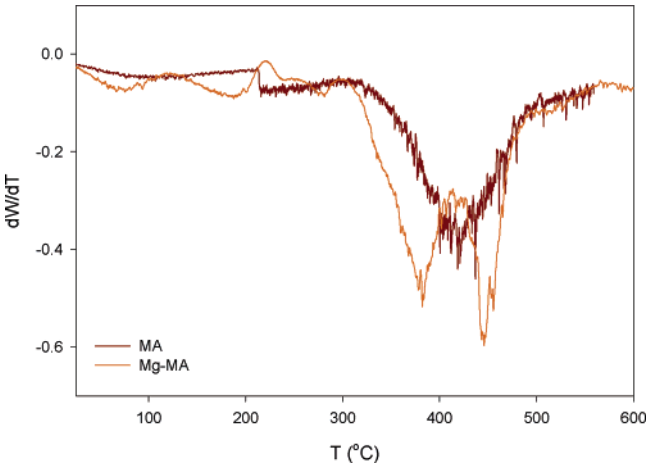

Figure 5. TGA patterns of MA and Mg-MA.

Table 2. Freundlich, Langmuir, Redlich−Peterson, Temkin, and Dubinin−Radushkevich Isotherm Constants for Nickel Ion Sorption on Mesoporous Alumina

isotherms	adsorbent = mesoporous alumina		
Freundlich isotherms	K_F (mg/g)	n	R^2
$q_e = K_F C_e^n$	16.642	0.175	0.920
Langmuir isotherms	$Q°$ (mg/g)	b (L/mg)	R^2
$q_e = Q^o b C_e/(1 + bC_e)$	22.321	8.615	0.988
Redlich−Peterson isotherm	K_R (L/g)	a_R (L/mg)	R^2
$q_e = K_R C_e/(1 + a_R C_e^\beta)$	9.931	2.175	0.968
Temkin isotherm	B	A (L/g)	R^2
$q_e = RT/(b \ln(AC_e))$	2.793	529.44	0.942
Dubinin−Radushkevich isotherm	q_s (mg/g)	E	R^2
$q_e = q_S \exp(-B\epsilon^2)$	20.452	3×10^{-8}	0.828

The constants K_F and n for Ni(II) and mesoporous alumina systems are presented in Table 2. The values of n lie between 1 and 10, indicating favorable adsorption.[23]

The Langmuir sorption isotherm is the best known of all isotherms describing sorption.[24] The Langmuir equation is applicable to homogeneous sorption, where the sorption of each sorbate molecule onto the surface has equal sorption activation energy. The Langmuir sorption isotherm is often used to describe sorption of a solute from a liquid solution as

$$\frac{1}{q_e} = \frac{1}{Q^o} + \frac{1}{bQ^o}\frac{1}{C_e} \tag{4}$$

where C_e is the equilibrium concentration (mg/L), q_e is the amount adsorbed at equilibrium (mg/g), and Q_0 and b are Langmuir constants related to adsorption capacity and energy of adsorption, respectively. The linear plots of $1/q_e$ vs $1/C_e$ show that the adsorption obeys the Langmuir isotherm model for mesoporous alumina and Ni(II) system. The values of Q_0 and b were determined from the slopes and the intercepts of the Langmuir plots and are represented in the Table 2.

Redlich and Peterson[25] incorporated the features of the Langmuir and Freundlich isotherms into a single equation and presented a general isotherm equation with a linear form as follows,

$$\frac{C_e}{q_e} = \frac{1}{K_R} + \frac{a_R}{K_R} C_e^\beta \tag{5}$$

where the exponent, β, lies between 0 (Henry's law equation) and 1 (Langmuir form). There are two limiting behaviors: Langmuir form for $\beta = 1$ and Henry's law form for $\beta = 0$. Plotting the C_e/q_e of the above equation against C_e^β to obtain the isotherm constants is not possible because of the three unknowns, a_R, K_R, and β. Therefore, a minimization procedure is adopted to solve the above equation by maximizing the correlation coefficient between the theoretical data for q_e predicted from the above equation and the experimental data. The Redlich−Peterson isotherm for the adsorption of Ni(II) onto mesoporous alumina and the constants and optimized values are presented in Table 2.

Temkin and Pyzhev[26] considered the effects of indirect adsorbate/adsorbate interactions on adsorption isotherms. The heat of adsorption of all the molecules in the layer would decrease linearly with coverage because of adsorbate/adsorbate interactions.

The Temkin isotherm has been used in the form as follows,

$$q_e = \frac{RT}{b} \ln A + \frac{RT}{b} \ln(C_e) \tag{6}$$

where $RT/b = B$.

The sorption data can be analyzed according to eq 6. Therefore, the linear plots of q_e vs $\ln C_e$ enable one to determine the constants A and b. The values of the Temkin constants A and B are listed in Table 2. The linear correlation coefficients are listed in Table 2, and from the table, the Temkin equation represents a better fit of the experimental data than the Freundlich and Langmuir equations, but not in the case of the Redlich−Peterson equation.

Another popular equation for the analysis of isotherms of a high degree of rectangularity is that proposed by Dubinin and Radushkevich (DR).[26]

$$\ln q_e = \ln q_S - B\epsilon^2 \tag{7}$$

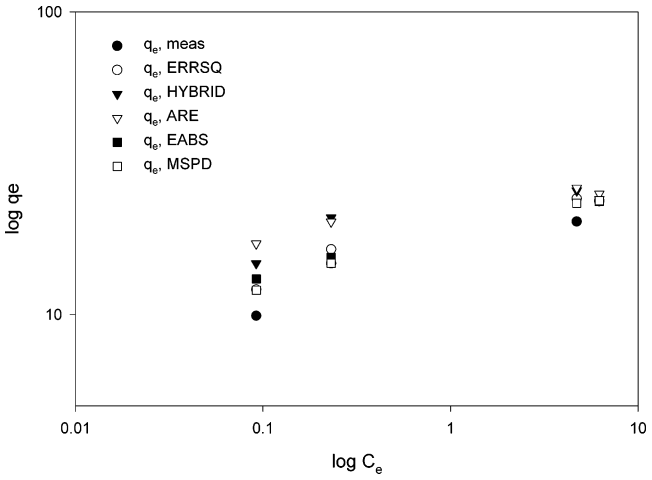

Figure 6. Error analysis for the Freundlich adsorption isotherm for Ni(II) and Mg-MA system.

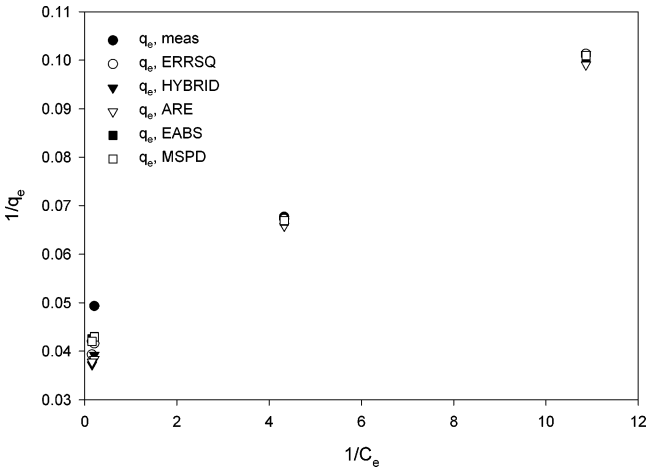

Figure 7. Error analysis for the Langmuir adsorption isotherm for Ni(II) and Mg-MA system.

where ϵ can be correlated as follows:

$$\epsilon = RT \ln\left[1 + \frac{1}{C_e}\right] \tag{8}$$

The constant B gives the mean free energy E of sorption per molecule of the sorbate when it is transferred to the surface of the solid from infinity in the solution and can be computed using the following relationship[27]

$$E = \frac{1}{\sqrt{2B}} \tag{9}$$

where R is the gas constant (8.31 J/(mol K)) and T is the absolute temperature. Therefore, a plot of ln q_e vs ϵ^2 enables one to determine the constants q_e and E, represented in Table 2. The correlation coefficients have been determined and are shown in Table 2, and the values of the correlation coefficients are much lower than the other four isotherm values. In this case, the DR equation represents a poorer fit of experimental data than the other isotherm equations.

3.3. Error Analysis for Isotherm Studies. In the single-component isotherm studies, the optimization procedure requires an error function to be defined in order to be able to evaluate the fit of the isotherm to the experimental equilibrium data. In this study, five different error functions were examined, and in each case, the isotherm parameters were determined by minimizing the respective error function across the concentration range studied. The error functions studied were as follows.

3.3.1. Sum of the Squares of the Errors (ERRSQ). The sum of the squares of the errors method can be represented by the equation

$$\sum_{i=1}^{p} (q_{e,calc} - q_{e,meas})_i^2 \tag{10}$$

where $q_{e,calc}$ are the theoretical adsorbed solid-phase concentrations of nickel on mesoporous alumina, which have been calculated from the isotherm equations (eqs 3 and 4), and $q_{e,meas}$ are the experimentally determined adsorbed nickel concentrations obtained from eq 1 using the experimentally measured equilibrium nickel liquid-phase concentrations, C_e.

Although this is the most common error function in use, it has one major drawback. Isotherm parameters derived using this error function will provide a better fit as the magnitude of the errors and, thus, the squares of the errors increases, biasing the fit toward the data obtained at the high end of the concentration range.

3.3.2. Hybrid Fractional Error Function (HYBRID). This error function was developed by Ng et al.[28] to improve the fit of the sum of the squares of the errors at low concentrations by dividing it by the measured value. It also includes the number of degrees of freedom of the system—the number of data points, n, minus the number of parameters, p, of the isotherm equation—as a divisor:

$$\frac{100}{n-p} \sum_{i=1}^{n} \left[\frac{(q_{e,meas} - q_{e,calc})^2}{q_{e,meas}}\right]_i \tag{11}$$

3.3.3. Marquardt's Percent Standard Deviation (MPSD). This error function was used previously by a number of researchers in the field.[29] It is similar in some respects to a geometric mean error distribution modified according to the number of degrees of freedom of the system:

$$100 \sqrt{\frac{1}{n-p} \sum_{i=1}^{p} \left(\frac{(q_{e,meas} - q_{e,calc})^2}{q_{e,meas}}\right)_i} \tag{12}$$

3.3.4. Average Relative Error (ARE). This error function[30] attempts to minimize the fractional error distribution across the entire concentration range:

$$\frac{100}{n} \sum_{i=1}^{p} \left|\frac{q_{e,calc} - q_{e,meas}}{q_{e,meas}}\right|_i \tag{13}$$

3.3.5. Sum of the Absolute Errors (EABS). This approach is similar to the sum of the squares of the errors. Isotherm parameters determined using this error function would provide a better fit as the magnitude of the error increased, biasing the fit toward the high concentration data:

$$\sum_{i=1}^{p} |q_{e,calc} - q_{e,meas}|_i \tag{14}$$

Since all the experiments were carried out at m/V ratios of almost exactly g/dm^3, according to the formulation of the problem, both C_e and q_e contribute equally to weighting the error criterion for the model solution procedure. Hence, the difference in the sorbed-phase concentration reflects the dif-

Table 3. Single-Component Freundlich and Langmuir Isotherm Results for Nickel onto Mesoporous Alumina Using Various Error Functions

parameters	ERRSQ	HYBRID	MPSD	ARE	EABS
		Freundlich isotherm			
K_f	18.703	21.145	22.085	18.587	18.063
n	0.152	0.104	0.090	0.140	0.160
R^2	0.950	0.796	0.949	0.997	0.994
		Langmuir isotherm			
$Q°$	24.937	26.178	26.385	23.809	23.866
b	7.035	6.474	6.649	7.777	7.618
R^2	0.996	0.994	0.995	0.999	0.999

Scheme 1. Mechanism of Ni^{2+} Adsorption on Mg-Mesoporous Alumina

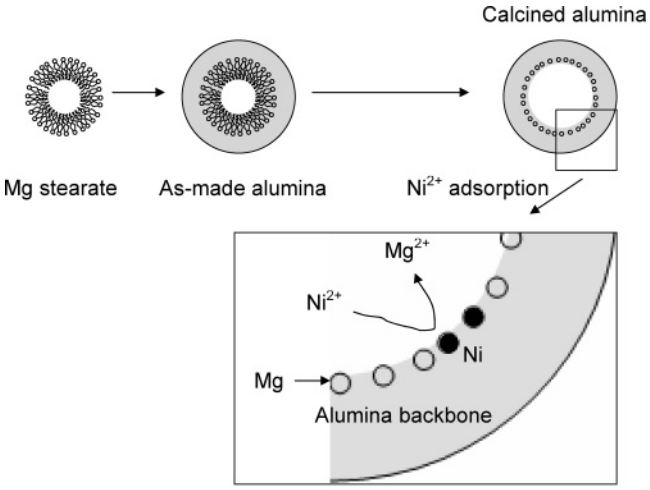

ferences in the predicted concentrations for both phases. From Figures 6 and 7, the EABS error function method provided the best parameters for the isotherm equations in the nickel−Mg-mesoporous alumina system, when the errors are being normalized for comparison purposes. The results for the error analyses are shown in Table 3 for Freundlich and Langmuir isotherms. From Table 3, the EABS has the highest R^2 values between different error function methods and is more significant. These data are used in the design of commercial adsorbers, and consequently, the more accurate the isotherm parameters, the more accurate are the system designs.

3.4. Adsorption Kinetic Modeling Studies. The kinetics of adsorption that describes the solute uptake rate governing the residence time of the sorption reaction is one of the important characteristics that defines the efficiency of sorption. Hence, in the present study, the kinetics of Ni(II) removal was carried out to understand the adsorption behavior of the prepared Mg-mesoporous alumina. Sorption of Ni(II) on mesoporous alumina involves a chemical sorption, which could control the reaction rate (Scheme 1). Therefore, the basis of this paper is to test the Ni(II) sorption using chemisorption pseudo-kinetic models. In order to investigate the mechanism of sorption, the rate constants of chemical sorption and intraparticle diffusion for the Ni(II) were determined using the equations of a pseudo-first-order system by Lagergren,[31] an intraparticle diffusion process by Weber and Morris,[32] and a pseudo-second-order mechanism, respectively. These are described as follows.

3.4.1. Pseudo-First-Order Kinetics. For the rate constant for pseudo-first-order chemical sorption,[33]

$$\log(q_e - q_t) = \log q_e - \frac{k_1}{2.303} t \qquad (15)$$

Table 4. Pseudo-First-Order Rate Constant and Intraparticle Diffusion Value at Different Initial Concentrations of Nickel Removal by Mesoporous Alumina

name of the resin	conc. of nickel (mg/L)	pseudo-first-order rate constant, k_1 (L/h)	intraparticle diffusion constant, k_{id} (mg/(g $h^{1/2}$))
mesoporous alumina	10	1.091	1.862
	20	0.157	1.488
	30	0.090	1.058

Table 5. Pseudo-Second-Order Rate Constant Value at Different Initial Concentrations of Nickel Removal by Mesoporous Alumina

sorbent name	concentration of copper (mg/L)	pseudo-second-order rate constant k_2 (g/(mg h))	R^2
mesoporous alumina	10	9.073	0.9999
	20	0.862	0.9997
	30	0.315	0.9977

the term k_1 (h^{-1}) is the first-order adsorption rate constant, q_e is the amount of metal adsorbed at equilibrium, and q_t is the amount adsorbed at time t. The first-order equation did not apply throughout all the contact times in this work. It was applicable over the initial 15−240 min sorption period. The plot of $\log(q_e - q_t)$ versus time at different adsorbate concentrations deviated considerably from the data after a short period. The calculated slopes and intercepts from the plots were used to determine the rate constant k_1 and the equilibrium capacity (q_e). The values of k_1, q_e, and regression coefficient are provided in Table 4.

3.4.2. Pseudo-Second-Order Kinetics. The rate of pseudo-second-order reaction may be dependent on the amount of solute sorbed on the surface of mesoporous alumina and the amount sorbed at equilibrium. The sorption equilibrium, q_e, is a function of, e.g., the initial metal ion concentration, the adsorbent dose, the particle size, and the nature of solute−sorbent interaction.

The kinetics of sorption of Ni(II) on Mg-mesoporous alumina were studied on the basis of the pseudo-second-order rate eq 16:[34]

$$\frac{t}{q_t} = \frac{1}{k_2 q_e^{\,2}} + \frac{t}{q_e} \qquad (16)$$

The product $k_2 q_e^2$ is the initial sorption rate h (eq 16)

$$\text{Rate} = k_2 q_e^{\,2} \qquad (17)$$

where k_2 (g/(mg h)) is the pseudo-second-order rate constant, q_e is the amount adsorbed at equilibrium, and q_t is the amount of Ni(II) adsorbed at time t. Plotting t/q_t against t at different adsobate concentrations (Figure 8) provided second-order sorption rate constant (k_2) and q_e values from the slopes and intercepts (see Table 5). The correlation coefficients (R^2) for these plots are superior. From Table 5, it was observed that the pseudo-second-order rate constant (k_2) decreased with increased initial concentration, and the initial sorption rate (h) was found to increase with increased initial Ni(II) concentration. The calculated q_e values agree very well with the experimental values, and a regression coefficient shows that the model can be applied for the entire adsorption process and confirms the chemisorptions of Ni(II) onto Mg-mesoporous alumina.

3.5. Effect of Contact Time and Initial Concentration. Figure 9 shows the effect of agitation time on the removal of nickel ions by Mg-mesoporous alumina. The results show that an increase in the initial nickel produces a reduction in the

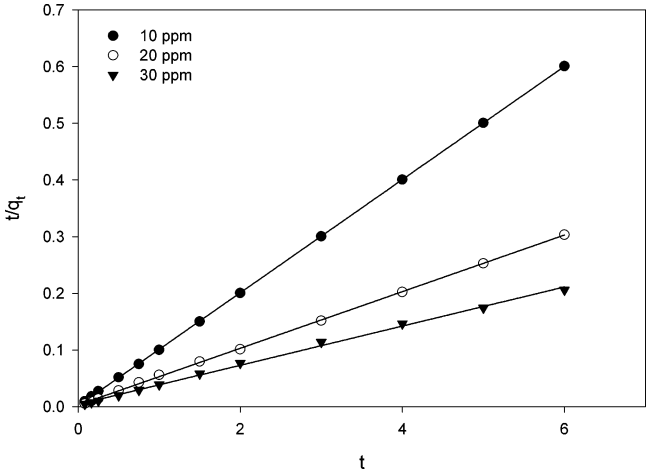

Figure 8. Pseudo-second-order kinetic fit for the adsorption of Ni(II) onto Mg-MA.

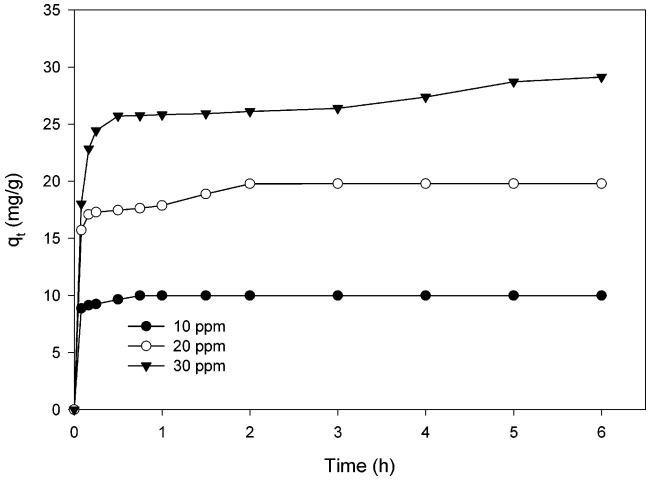

Figure 9. Agitation time on the removal of nickel ions by Mg-mesoporous alumina. [conditions: amount of Mg-MA = 1 g/L; pH = 4.8].

percentage of Ni(II) ions from the aqueous solution. The removal of Ni(II) decreases from 99% to 97% with the increase of initial Ni(II) ion concentration from 10 to 30 mg/L at pH. 4.8, showing the process to be highly dependent on the initial concentration. The rate constants K_2, obtained from the plots of eq 16, are shown in Table 4. Figure 8 shows a plot of the linearized form of the model in eq 16 for the sorption of Ni(II) onto mesoporous alumina at different initial Ni(II) ion concentrations. Table 5 also indicates that the regression coefficients for the linear plots from the pseudo-second-order equation are >0.9999 for all the systems.

The nature of the rate-limiting step in a batch system can be assessed from the properties of the solute and sorbent. Weber and Morris[32] stated that, if intraparticle diffusion is the rate-controlling factor, uptake of the sorbate varies with the square root of time. Thus, rates of sorption are usually measured by determining the change in concentrations of sorbate with the sorbent as a function of the square root of time, and the k_{id} values are presented in Table 4. Figure 10 shows the amount of sorption against the square root of time, and the straight lines do not pass through the origin; therefore, intraparticle diffusion also may not be the sole rate-limiting factor.[35] Poots et al.[36] proposed that, during the early stages of sorption, some boundary-layer resistance was involved. However, for the sorption of Ni(II) ions onto mesoporous alumina, the linearized plots of eq 16 have a good correlation of the data shown in Figure 8. The correlation coefficients, r^2, for the pseudo-second-

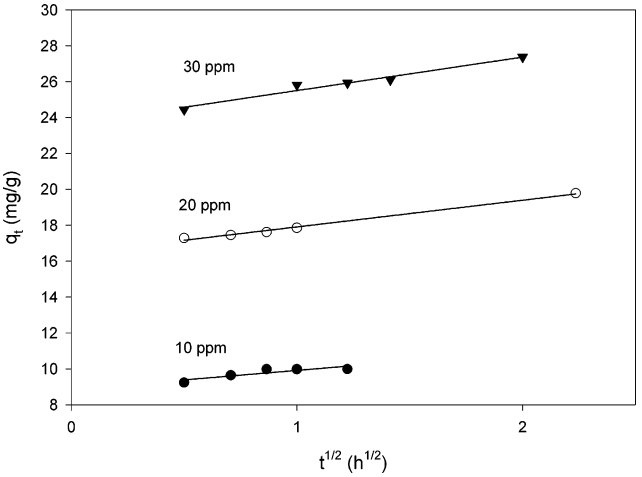

Figure 10. Intraparticle diffusion plot for the adsorption of Ni(II) on Mg-MA.

order kinetic model are much greater than the intraparticle diffusion coefficients for the sorption/reaction of Ni(II) ions onto mesoporous alumina (Scheme 1), strongly suggesting a chemical reaction mechanism. The overall rate of the sorption process appears to be controlled by the chemical process in the case of Ni(II), in accordance with the pseudo-second-order reaction mechanism.

In order to find out the validity of kinetic model for the pseudo-second-order adsorption kinetics of Ni(II) onto the prepared Mg-MA, it was verified at different initial concentrations. The validity of each model was determined by the sum of squared errors, and the calculated values are 0.48%, 6.76%, and 12.36% for 10, 20, and 30 ppm of Ni(II), respectively. It was found that the adsorption of Ni(II) onto the Mg-MA could be best described by the pseudo-second-order kinetic model. This equation is based on the equilibrium chemical adsorption, which predicts the behavior over the whole range of studies, strongly supporting the validity, and agrees with chemisorptions being rate-controlling.[37]

4. Conclusion

The studies presented revealed that the Mg-mesoporous alumina can be fruitfully employed as adsorbents for the Ni(II) removal because the ΔG value of Mg(II), which is present in mesoporous alumina, has a more negative value when compared with Ni ion. The percentage of Ni(II) removal from 10 ppm solution by these Mg-MA is >99%. The equilibrium sorption isotherm of Ni(II) onto Mg-MA has been analyzed by Freundlich, Langmuir, Redlich−Peterson, Temkin, and Dubinin−Radushkevich isotherm equations. The EABS error function provides the best parameters for the isotherm equation in this system. The isotherm parameters are different from those values obtained using linearized data analysis and must be considered to be more accurate for application in the design of commercial adsorbers. Furthermore, different values of the Freundlich and Langmuir isotherm constants are obtained using the different error analysis methods. This is a significant conclusion, even though the constants from the linear and nonlinear error analysis are quite close. The adsorption of Ni(II) onto Mg-MA was well-fitted with the pseudo-second-order kinetic model. This work shows the interest of a concept based on the use of this material to treat waste or to resolve an environmental problem. This method can be used as an alternative to the conventional methods. It also can be employed for the recovery of metal traces and/or polishing of treated effluents.

Acknowledgment

S.R. gratefully acknowledges the Brain Pool program of Korea Science and Engineering Foundation for financial support to carry out this work. Y.K. is grateful to the Research Grant of Kwangwoon University in 2006 for financial support.

Nomenclature

A = Temkin isotherm constant related to adsorbate/adsorbate interaction (L/g)
a_R = constant of Redlich−Peterson isotherm (L/mg)
B = Temkin isotherm constant
b = Langmuir constant (L/mg)
C_e = equilibrium adsorbate concentration (mg/L)
C_o = initial concentration of adsorbate (mg/L)
C_t = solution phase adsorbate concentration at time t (mg/L)
E = Dubinin−Radushkevich isotherm constant
k_1 = rate constant of pseudo-first-order adsorption model (L/h)
k_2 = rate constant of pseudo-second-order adsorption model (g/(mg h))
K_F = Freundlich constant (mg/g)
k_{id} = intraparticle diffusion rate constant (mg/(g $h^{1/2}$))
K_R = constant in Redlich−Peterson isotherm (L/g)
M = mass of the adsorbent (g)
Mg-MA = magnesium mesoporous alumina
n = Freundlich isotherm constant related to adsorption intensity
N = number of data points
q_e = equilibrium adsorption uptake concentration (mg/g)
$q_{e,cal}$ = calculated value of adsorbate concentration at equilibrium (mg/g)
$q_{e,exp}$ = experimental value of adsorbate concentration at equilibrium (mg/g)
q_{max} = maximum adsorption capacity of adsorbent (mg/g)
$Q°$ = Langmuir constant (mg/g)
q_s = Dubinin−Radushkevich isotherm constant related to adsorption capacity (mg/g)
q_t = amount of adsorbate adsorbed by adsorbent at time t (mg/g)
R = universal gas constant (8.314 J/(K mol))
R^2 = correlation coefficient
T = absolute temperature (K)
t = time (h)
V = volume of the solution (L)
β = constant of Redlich−Peterson isotherm ($0 < \beta < 1$)

Literature Cited

(1) Ko, D. C. K.; Porter, J. F.; McKay, G. Optimised correlations for the fixed bed adsorption of metal ions on bone char. *Chem. Eng. Sci.* **2000**, *55*, 5819−5829.

(2) Rengaraj, S.; Yeon, K.-H.; Moon, S. H. Removal of nickel from water and synthetic nuclear power plant coolant water by ion exchange resins. *J. Radioanal. Nucl. Chem.* **2002**, *252*, 241−245.

(3) Xu, H.; Liu, Y.; Tay, J. H. Effect of pH on nickel biosorption by aerobic granular sludge. *Bioresour. Technol.* **2006**, *97*, 359−363.

(4) Beliles, R. P. The lesser metals. In *Toxicity of Heavy Metals in the Environment, Part 2*; Oehme, F. W., Ed.; Marcel Decker: New York, 1979; p 583.

(5) Parker, S. P. *Encyclopedia of Environmental Sciences*, 2nd ed.; McGraw Hill: New York, 1980.

(6) Peryasamy, K.; Namasivayam, C. Removal of Nickel(II) from aqueous solution and nickel plating industry wastewater using an agricultural waste: Peanut Hulls. *Waste Manage.* **1995**, *15*, 63−68.

(7) EPA. *Summary Report: Control and treatment technology for the metal finishing industry: Ion exchange*; EPA 625/8-81-007; EPA: Cincinnati, OH, 1981.

(8) Dean, J. G.; Bosqui, F. L.; Lanouette, K. H. Removing heavy metals from wastewater. *Environ. Sci. Technol.* **1972**, *6*, 518−522.

(9) McAnally, S. L.; Benefield, T.; Reed, R. B. Nickel removal from a synthetic nickel plating wastewater using sulphide and carbonate for precipitation and coprecipitation. *Sep. Sci. Technol.* **1984**, *19*, 191−217.

(10) Nilsson, R. Removal of metals by chemical treatment of municipal wastewater. *Water Res.* **1971**, *5*, 51−61.

(11) Akhtar, N.; Iqbal, J.; Iqbal, M. Removal and recovery of nickel(II) from aqueous solution by loofa sponge immobilized biomass of chlorella sorokiniana: Characterization studies. *J. Hazard. Mater.* **2004**, *108*, 85−94.

(12) Al-Dalama, K.; Aravind, B.; Stanislaus, A. Influence of complexing agents on the adsorption of molybdate and nickel ions on alumina. *Appl. Catal., A* **2005**, *296*, 49−53.

(13) Hong, K. M.; Kim, M. S.; Chung, J. G. Adsorption characteristics of Ni(II) on γ-type alumina particles and its determination of overall adsorption rate by a differential bed reactor. *Chemosphere* **2004**, *54*, 927−934.

(14) Kim, Y.; Kim, C.; Choi, I.; Rengaraj, S.; Yi, J. Arsenic removal using mesoprous alumina prepared via a templating method. *Environ. Sci. Technol.* **2004**, *38* (3), 924−931.

(15) Rengaraj, S.; Kim, Y.; Joo, C. K.; Yi, J. Removal of copper from aqueous solution by aminated and protonated mesoporous aluminas: kinetics and equilibrium. *J. Colloid Interface Sci.* **2004**, *273*, 14−21.

(16) Kim, C.; Kim, Y.; Kim, P.; Yi, J. Synthesis of mesoporous alumina using a cost-effective template. *Korean J. Chem. Eng.* **2003**, *20* (6), 1142−1144.

(17) Kim, Y.; Lee, B.; Yi, J. Synthesis of mesoporous gamma-alumina through pre- and post-hydrolysis methods. *Korean J. Chem. Eng.* **2002**, *19* (5), 908−910.

(18) Kim, Y.; Kim, C.; Choi, J. W.; Kim, P.; Yi, J. Synthesis of Mesoporous Gamma-Aluminas of Controlled Pore Properties Using Alkyl Carboxylate Assisted Method. *Stud. Surf. Sci. Catal.* **2003**, *146*, 209−212.

(19) Kim, Y.; Kim, P.; Kim, C.; Yi, J. Comparison of mesoporous aluminas synthesized using stearic acid and its salts (Na, Mg, and Ni). *Korean J. Chem. Eng.* **2005**, *22* (2), 321−327.

(20) Kim, Y.; Kim, C.; Kim, P.; Yi, J. Effect of Preparation Conditions on the Phase Transformation of Mesoporous Alumina. *J. Non-Cryst. Solids* **2005**, *351* (6−7), 550−556.

(21) Kim, Y.; Lee, B.; Yi, J. Effects of framework and textural porosities of functionalized mesoporous silica on metal ion adsorption capacities. *Sep. Sci. Technol.* **2004**, *39*, 1427−1442.

(22) Kim, Y.; Kim, P.; Kim, C.; Yi, J. A novel method for synthesis of a Ni/Al_2O_3 catalyst with a mesoporous structure using stearic acid salts. *J. Mater. Chem.* **2003**, *13*, 2353−2358.

(23) Slejko, F. A step by step approach to process evaluation and application. In *Adsorption Technology*; Marcel Dekker: New York, 1985.

(24) Coskun, R.; Soykan, C.; Sacak, M. Adsorption of copper(II), nickel-(II) and cobalt(II) ion from aqueous solution by methacrylic acid/acrylamide monomer mixture grafted poly(ethylene terephthalate) fiber. *Sep. Purif. Technol.* **2006**, *49*, 107−114.

(25) Srivastava, V. C.; Mall, I.; Mishra, I. M. Equilibrium modeling of single and binary adsorption of cadmium and nickel onto bagasse fly ash. *Chem. Eng. J.* **2006**, *117*, 79−91.

(26) Choy, K. K. K.; McKay, G.; Porter, J. F. Sorption of acid dyes from effluents using activated carbon. *Resour., Conserv. Recycl.* **1999**, *27*, 57−71.

(27) Hasany, S. M.; Chaudhary, M. H. Sorption potential of Hare river sand for the removal of antimony from acidic aqueous solution. *Appl. Radiat. Isot.* **1996**, *47*, 467.

(28) Ng, J. C. Y.; Cheung, W. H.; McKay, G. Equilibrium studies of the sorption of Cu(II) ions onto chitosan. *J. Colloid Interface Sci.* **2002**, *255*, 64−74.

(29) Seidel, A.; Gelbin, D. On applying the ideal adsorbed solution theory to multicomponent adsorption equilibria of dissolved organic components on activated carbon. *Chem. Eng. Sci.* **1988**, *43*, 79−88.

(30) Kapoor, A.; Yang, R. T. Correlation of equilibrium adsorption data of condensable vapours on porous adsorbents. *Gas Sep. Purif.* **1989**, *3*, 187−192.

(31) Lagergren, S.; Venska, B. K. Zur theorie der sogenannten adsorption geloester stoffe. *Vaternskapsakad Handlingar* **1898**, *24*, 1−39.

(32) Akkaya, G.; Uzun, I.; Guzel, F. Kinetcis of the adsorption of reactive dyes by chitin. *Dyes Pigm.* **2007**, *73*, 168−177.

(33) Ho, Y. S.; McKay, G. A kinetic study of dye sorption by biosorbent waste product pith. *Resour., Conserv. Recycl.* **1999**, *25*, 171−193.

(34) Ho, Y. S.; McKay, G. Pseudo-second order model for sorption processes. *Process Biochem.* **1999**, *34*, 451−465.

(35) Poots, V. J. P.; McKay, G.; Healy, J. J. The removal of acid dye from effluent, using natural adsorbent. II. Wood. *Water Res.* **1976**, *10*, 1067−1070.

(36) Poots, V. J. P.; McKay, G.; Healy, J. J. The removal of acid dye from effluent, using natural adsorbent. I. Peat. *Water Res.* **1976**, *10*, 1061−1066.

(37) Tseng, R.-L.; Tseng, S.-K. Pore structure and adsorption performance of the KOH-activated carbons prepared from corncob. *J. Colloid Interface Sci.* **2005**, *287*, 428−437.

Received for review July 28, 2006
Revised manuscript received October 30, 2006
Accepted January 3, 2007

IE060994N